



The precessional phase lag of Messinian gypsum deposition in Mediterranean marginal basins

R.P.M. Topper*, P.Th. Meijer

Department of Earth Sciences, Utrecht University, Budapestlaan 4 3584CD Utrecht, The Netherlands

ARTICLE INFO

Article history:

Received 7 January 2014

Received in revised form 14 October 2014

Accepted 19 October 2014

Available online 28 October 2014

Keywords:

Messinian Salinity Crisis

Modelling

Phase lag

Mediterranean

Precession

Chronostratigraphy

ABSTRACT

The uncertainty of the phase relation between the forcing and sedimentary expression is yet unquantified, introducing a bias in tuning recurrent facies variations in the sedimentary record to the astronomical forcing. The identification of a phase lag between precession and the most recent sapropel in the Mediterranean demonstrates that astronomical forcing and its sedimentary expression are not always in phase. Gypsum deposition in Mediterranean marginal basins during the Messinian Salinity Crisis is also forced by precession-driven climate changes. In contrast to sapropel formation, which involves complex interactions of circulation and biogeochemistry, gypsum formation in such basins is primarily controlled by salinity. Using a simple box model to represent the Late Miocene Mediterranean, we examine the phase relation between gypsum deposition and precessional forcing. For a large range of settings model results show a consistent phase lag between the precessional forcing and salinity in the marginal and deep basins of the Mediterranean. On the basis of our quantitative modelling results we propose that in the astronomical tuning of the Messinian gypsum deposits, a phase lag of $3.3 \text{ kyr} \pm 2.6 \text{ kyr}$ should be taken into account for cycles with a duration of 20 kyr. Accordingly, the astronomically tuned ages of the gypsum deposits become, on average, 3.3 kyr younger. In the anomalously short 14 kyr cycle that follows the onset of the Messinian Salinity Crisis the phase lag is smaller and within range of the other uncertainties of astronomical tuning.

© 2014 Elsevier B.V. All rights reserved.

1. Introduction

A progressive restriction of the Atlantic–Mediterranean connection(s) was the main driver of an increasing salt concentration in the Mediterranean in the Late Miocene (e.g. Krijgsman et al., 1999; Kouwenhoven and van der Zwaan, 2006; CIESM, 2008). In the sedimentary record, the increasing salinity is demonstrated by the occurrence of gypsum deposits in former marginal basins throughout the Mediterranean. The interval in which these gypsum deposits were formed is the first phase, the Primary Lower Gypsum (PLG) phase, of the event known as the Messinian Salinity Crisis (MSC; Krijgsman et al., 1999; CIESM, 2008). A further restriction of the Atlantic–Mediterranean gateways eventually led to the deposition of kilometre-thick sequences of halite in deep Mediterranean basins during the second phase of the MSC. A third phase characterized by local evaporite deposits in an overall brackish water environment, caused by a significant change in the fresh water budget of the Mediterranean, concluded the MSC before a return to normal marine conditions in the Pliocene.

Within the PLG deposits, cyclic alternations of organic-rich shale and gypsum are evidence for changes in the basinal salt concentration on a

shorter timescale. Similar cyclic alternations of sapropel and marl, with often an intercalation of diatomite, in pre-MSC sequences have been linked to precession-driven changes in the circum-Mediterranean climate and have been used to derive an astronomically tuned time scale for the pre-MSC sequences. The recent development of a robust stratigraphic framework for the PLG deposits has allowed the definitive extension of the cyclostratigraphic framework from the pre-MSC into the MSC (Lugli et al., 2010; Manzi et al., 2013). In the pre-MSC and PLG sequences, respectively, sapropel and shale layers are correlated with insolation maxima (precession minima), during which river runoff and precipitation are close to or exceed evaporation (Krijgsman et al., 1999; Lugli et al., 2010). Marls and gypsum layers are correlated with insolation minima (precession maxima), during which evaporation exceeds precipitation and river runoff.

Although it is generally assumed that orbital forcing and its sedimentary expression are in phase, their phase relation is an important source of uncertainty in astronomically tuned time scales. Other uncertainties in astronomical tuning derive from uncertainties in the dynamical ellipticity of the Earth and the tidal dissipation by the Moon in the astronomical solution. These uncertainties have been estimated to be 1–2 kyr for the last 7 Myr, based on the good correspondence between the astronomical solution and sapropel patterns in the Mediterranean (Rivera et al., 2011). For the Mediterranean in the Quaternary, climate models show that the boreal summer monsoon, thought to be the main

* Corresponding author at: MARUM — Center for Marine Environmental Sciences and Department of Geosciences, University of Bremen, PO Box 33 04 40, D-28334, Germany. Tel.: +49 421 218 65455.

E-mail address: rtopper@marum.de (R.P.M. Topper).

driver of sapropel formation, is in phase with the precession signal (Tuenter et al., 2005; Kutzbach et al., 2008; Weber and Tuenter, 2011). The most recent sapropel, S1, however, lags 3 kyr with respect to the corresponding precession minimum (Lourens et al., 1996); a lag that still has not been fully explained (e.g. Lourens et al., 1996; Ziegler et al., 2010). None of the orbitally tuned time scales for the Miocene, and hence the Messinian, have taken any phase lag of sapropels into account. Sapropel midpoints are correlated with precession minima. Precession maxima are correlated with marl or gypsum layer midpoints, or the change from massive/banded selenite to branching selenite sensu Lugli et al. (2010). For the Messinian, Krijgsman et al. (1999) mentioned an uncertainty of one precession cycle (20 kyr) in the astronomically tuned ages, derived from an uncertainty in the correlation with the astronomical solution. In the recent revision of Manzi et al. (2013), only the uncertainties due to dynamical ellipticity, tidal dissipation, and the precession phase of the sedimentary expression are retained.

In order to examine the phase relation of sapropel formation in the Mediterranean to precession, a transient run with a fully-coupled high-resolution climate model is necessary to resolve changes in Mediterranean circulation and biogeochemistry (e.g. Adloff et al., 2011; Grimm, 2012). The precession phase of gypsum deposition during the PLG, on the other hand, is easier to determine because deposition took place in marginal instead of deep Mediterranean basins. Furthermore, the main controlling parameter is the basinal salinity which is readily calculated, and gypsum deposition in marginal basins is, to our knowledge, not significantly affected by biochemical processes. In this study, we will use a simple box model set up to represent the Late Miocene Mediterranean, forced with a precessionally varying fresh water budget, to examine the precessional phase of the gypsum deposits of the MSC. Model results will be checked for sensitivity to the fresh water budget, the size of the Atlantic gateway(s) and the degree of water column stratification since these are uncertain for the PLG phase. Any precession lag found has direct consequences for the astronomical tuning of the PLG sequences (ages and uncertainty) and the timing of the onset of the MSC.

2. Model description

Box models have recently been used to represent the Late Miocene Mediterranean in a number of studies which quantitatively examined various hypotheses regarding the Messinian Salinity Crisis (Meijer, 2006; Topper et al., 2011; Topper and Meijer, 2013; Topper et al., 2014). The model used in this study closely resembles that of Topper et al. (2014) in their default setup. The Mediterranean is represented by two boxes: one box represents the deep basins of both the western and eastern Mediterranean, valid under the assumption that interbasinal exchange was large enough to keep water characteristics in both basins equal (see Topper and Meijer, 2013), and the other represents a generic marginal basin (Fig. 1A). The Atlantic, represented by a box with constant water characteristics, is connected to the deep Mediterranean basin box. Outflow from the deep and marginal basin to, respectively, the Atlantic and deep basin is parameterized as linearly proportional to the density difference between the basins. Density is solely determined by the salinity, temperature being neglected following Topper et al. (2011). Factors of proportionality, g_{DA} (deep basin to Atlantic) and g_{MD} (marginal to deep basin), are used to derive the outflow from the density difference. A factor of $\approx 10^5 \text{ m}^3 \text{ s}^{-1} (\text{g L}^{-1})^{-1}$ represents the present-day Strait of Gibraltar, lower factors represent more restricted gateways (units of these factors will be dropped in the remainder of this article). An inflow compensates for the outflow and the fresh water deficit or excess, i.e. evaporation–precipitation–river runoff ($E-P-R$), to keep basinal volumes constant. We deliberately leave out sea level (volume) changes because our focus is on the atmospheric expression of the precessional forcing. Moreover, including it would add additional complexity to the results well beyond the scope of this study.

The model employs a Late Miocene fresh water budget which has been derived from the results of Gladstone et al. (2007). Evaporation minus precipitation ($E - P$) is 1 m/yr and total river runoff (R) is $41.6 \cdot 10^3 \text{ m}^3 \text{ s}^{-1}$ (Table 1). Compared to the present-day Mediterranean fresh water budget both $E - P$ and R are higher; $E-P-R$, however, is similar in magnitude (0.5 m/yr). More details and a discussion of the applicability of this water budget can be found in Topper et al. (2011).

A change in the river discharge can be imposed by multiplying the Late Miocene reference value with the factors fR_D and fR_M for respectively the river runoff in the deep and marginal basins (Fig. 1B).

The variation of the fresh water budget during a precession cycle is defined as a sinusoidal variation of R and $E - P$. This representation of precessional water budget variation is based on the results of climate model studies which show that (1) R and $E - P$ variations are in phase with the precession signal, and (2) the variation is proportional to the magnitude of the precession signal modulated by eccentricity (Tuenter et al., 2005; Kutzbach et al., 2008; Weber and Tuenter, 2011). The amplitude of variation is controlled by $ampR$ and $ampE$. These amplitudes are expressed as a percentage of the average R and $E - P$, i.e. the fresh water budget varies between $(1 - ampE) \cdot (E - P)_{ref} - (1 + ampR) \cdot fR \cdot R_{ref}$ and $(1 + ampE) \cdot (E - P)_{ref} - (1 - ampR) \cdot fR \cdot R_{ref}$. Higher $ampR$ and $ampE$ thus correspond to a precession cycle with a larger amplitude and vice versa. The period of the sinusoidal variation is 20 kyr, an idealized length in between the two dominant precession frequencies (19–23 kyr). In each precession cycle, maximum R and minimum $E - P$ correspond to the precession minimum, minimum R and maximum $E - P$ with the precession maximum, i.e. precession is exactly in phase or in antiphase with the two components of the fresh water budget.

Total salinity (S), gypsum (CaSO_4) and halite (NaCl) concentrations are the parameters the model solves for in both the marginal and deep basin boxes. The model is initialized with the salt concentrations used for the Atlantic box (Table 1). A parametrization of water column stratification is included in the model; the factor fL is used to set the degree of water column stratification. With $fL = 0$, surface and deep water salinities are equal; with any higher $xtitfL$ (up to $fL = 1$), surface water becomes less saline while deep layer salinities are higher. Basin average salinity is, however, not affected by the degree of stratification.

Without stratification, if gypsum and/or halite concentrations exceed their respective saturation concentrations, all gypsum/halite in excess of saturation in the whole basinal volume is deposited. With stratification, the deep water layer will always reach saturation before the surface layer. Therefore, only the gypsum/halite in excess of saturation in the deep water layer will be deposited. More details on the algorithms used for stratification and evaporite deposition can be found in Topper and Meijer (2013).

An extensive analysis of the sensitivity of model results to marginal basin volume, surface area and river input has been conducted in Topper et al. (2014). The influence of these parameters is minor compared to the influence of gateway sizes and fresh water budget. Hence, we adopt the default values for these parameters from Topper et al. (2014): the marginal basin has a surface area of 0.05% and a volume of 0.01% of the total Mediterranean surface area and volume, i.e. $\approx 1200 \text{ km}^2$ and 375 km^3 (depth of 300 m), and gets 0.1% of the total Mediterranean river input. The marginal basin size in the model is in the order of magnitude thought to be appropriate for the Vena del Gesso, Sorbas, and Sicilian wedge-top basins. Parameters that will be varied in the results presented here, are (1) the size of the Atlantic–Mediterranean connection (g_{DA}), (2) the size of the marginal–deep basin connection (g_{MD}), (3) the average river discharge during a precession cycle (fR 's), and (4) the amplitude of variation of the fresh water budget during a precession cycle ($ampR$ and $ampE$).

Regardless of the setup, a dynamic equilibrium is reached within 1 Myr, i.e. minimum and maximum values of total salt, gypsum and halite concentrations are constant in consecutive precession cycles. Results in the next sections are derived from the last 50 kyr (2.5 precession cycles) of each 1 Myr model run.

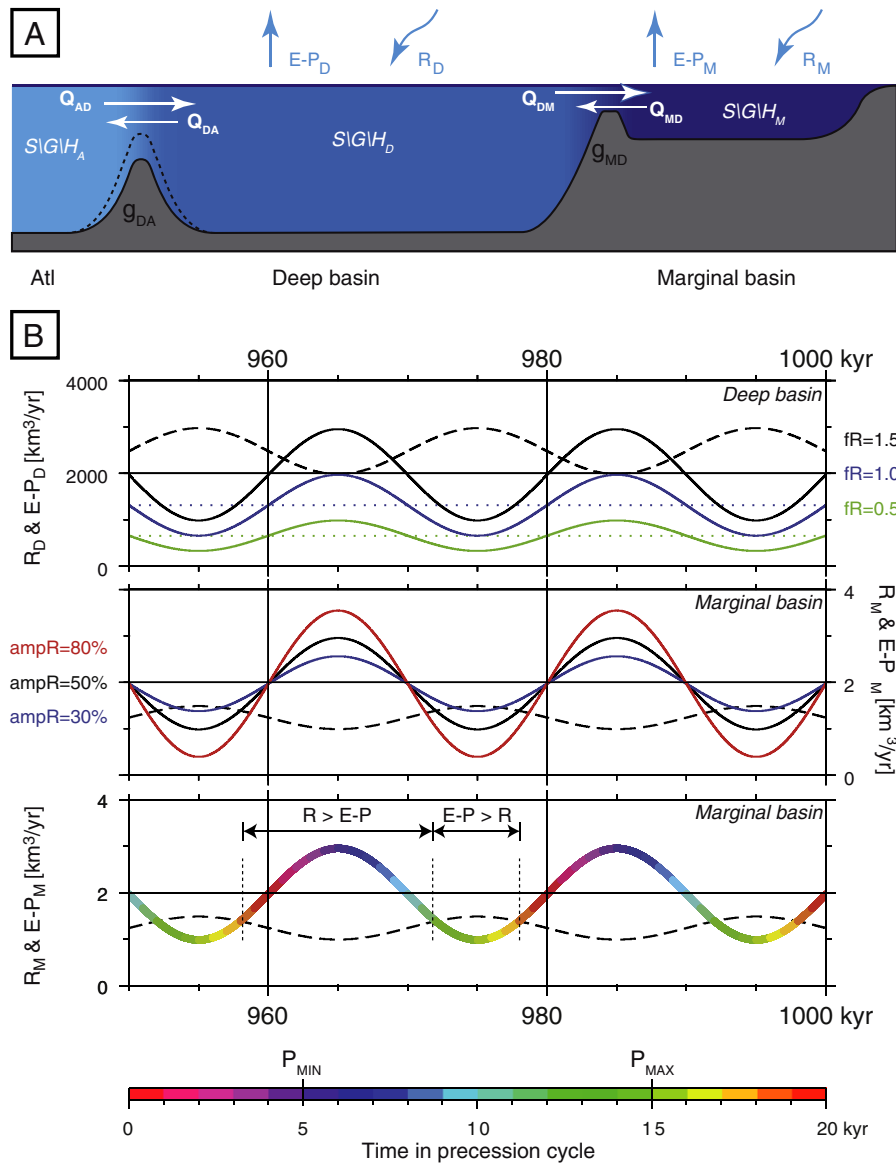


Fig. 1. (A) Graphic representation of the box model. White arrows indicate volume fluxes (Q 's) between the basins, the first subscript character represents the source, the second one the destination. The fresh water budget consists of: $E - P_D$ and $E - P_M$, evaporation minus precipitation, and R_D and R_M , river discharges. $S(\text{alinity})/C(\text{gypsum concentration})/H(\text{alite concentration})_x$ are the water characteristics of the respective basins (indicated by x). (B) Fresh water forcings, R (solid line) and $E - P$ (dashed line), for the deep basin (top frame) and marginal basin (middle frame) during 2.5 precession cycles (50 kyr, ending at the model run time of 1 Myr). The effect of a change in fR on the river discharge is demonstrated in the top frame where dotted lines indicate the precession-averaged river discharge. The effect of $\text{amp}R$ is demonstrated in the middle frame. The bottom frame indicates the intervals of $E - P > R$ and $R > E - P$. The colour of the R_M curve indicates the time within a precession cycle.

3. Results

3.1. A causal mechanism for phase lags

For the purpose of illustrating the main factors that affect the timing of salt concentration extrema in the deep and marginal basin, model parameters have been chosen such that a distinct evolution of water characteristics in deep and marginal basins exists and gypsum saturation is reached only in the marginal basin (Fig. 2; $fR_D = 1.5$, $fR_M = 1.5$, $\text{amp}R = 50\%$, $\text{amp}E = 20\%$, $g_{DA} = 10^2$, $g_{MD} = 10^0$, $fL = 0$). Although set up for illustrative purposes, the model behaviour in this specific setup is representative of the generic behaviour in a larger range of settings.

In Fig. 2C, the precession-driven sinusoidal forcing of R and $E - P$ is shown for both the marginal and deep basins. On average, the deep basin has a negative fresh water budget, i.e. $E - P > R$. However, due to the cyclic variation of $E - P$ and R , an interval in each cycle exists where $R > E - P$ (the interval between the blue vertical dashed lines in

Fig. 2). Because on average $E - P$ exceeds R , the time interval with $E - P > R$ is longer than the interval with $R > E - P$ (12.250 vs 7.750 kyr). Also, the intersections of the $E - P$ and R curves, where the net fresh water budget ($E - P - R$) goes from positive to negative or vice versa, are further from the maximum in $E - P$ than from the minimum in R , and are closer to the minimum in $E - P$ than to the minimum in R . For the marginal basin, R exceeds $E - P$ on average and the pattern is reversed; the interval with $R > E - P$ is longer than the interval with $E - P > R$ (14.020 vs 5.980 kyr) and intersections are closer to the maximum in $E - P$ and the minimum in R .

The net transport, in or out of the marginal basin, is equal to the net fresh water budget of the marginal basin, i.e. marginal $E - P - R$ in Fig. 2C equals the net flow in Fig. 2F. The net transport is positive for net inflow to the marginal basin when $E - P > R$ (during 5.980 kyr), and negative for net outflow from the marginal basin when $R > E - P$ (during 14.020 kyr). The net transport between the Atlantic and deep basin is equal to the net fresh water budget of the deep and marginal basins

Table 1
Overview of parameter values used to set up the model.

Parameter	Detail	Value	Reference
<i>Mediterranean volume/surface area</i>			
V	Late Miocene volume	$3750.7 \cdot 10^{12} \text{ m}^3$	Meijer et al. (2004)
A	Late Miocene surface area	$2.4780 \cdot 10^{12} \text{ m}^2$	Meijer et al. (2004)
<i>Messinian fresh water fluxes</i>			
E – P	Evaporation–precipitation	1 m yr^{-1}	Gladstone et al. (2007)
R _{west}	River input in WMed	$5526.4 \text{ m}^3 \text{ s}^{-1}$	Gladstone et al. (2007)
R _{east}	River input in EMed	$36067.4 \text{ m}^3 \text{ s}^{-1}$	Gladstone et al. (2007)
<i>Salinity</i>			
S _A	Ocean water	35 kg m^{-3}	
S _R	River input	0 kg m^{-3}	
<i>Gypsum (CaSO₄)</i>			
G _A	Ocean water	1.27 kg m^{-3}	Leeder (1999)
G _R	River input	0 kg m^{-3}	
G _{SAT}	Gypsum saturation	5.25 kg m^{-3}	
<i>Halite (NaCl)</i>			
H _A	Ocean water	27.21 kg m^{-3}	Leeder (1999)
H _R	River input	0 kg m^{-3}	
H _{SAT}	Halite saturation	272.1 kg m^{-3}	

(Fig. 2D). Even though the marginal fresh water budget is small compared to that of the deep basin, it does affect the exchange with the Atlantic. The interval with net outflow from the Mediterranean is slightly longer than the interval where $R > E - P$ in the deep basin (7.760 vs 7.750 kyr), i.e. in between the lengths of the $R > E - P$ intervals of deep and marginal basins (in between blue and red dashed lines).

Salinity in the deep basin (Fig. 2A) increases in the $E - P > R$ interval during which a net inflow to the Mediterranean exists. The net inflow brings Atlantic water to the Mediterranean, of this inflow the water evaporates and the salt is left in the Mediterranean. With increasing salinity, the density driven outflow grows both in volume (Fig. 2D) and salt transport (Fig. 2E). At a certain point in the $E - P > R$ interval, the amount of salt in the inflow equals the amount of salt in the outflow (959.170 kyr, intersection of lines in Fig. 2E). In the remainder of the $E - P > R$ interval, more salt leaves the Mediterranean with the outflow than comes in with the inflow which is still larger in volume. Consequently, the maximum salinity in the Mediterranean is reached before the net inflow switches to a net outflow (1.930 kyr before the intersection of the $E - P_D$ and R_D curves in Fig. 2C). Salinities in the deep basin continue to drop in the $R > E - P$ interval, the net outflow transports salt from the Mediterranean to the Atlantic. When salinity in the deep basin drops below the Atlantic salinity, the reversed density difference drives a deep inflow of Atlantic water while a larger outflow at the surface persists. In the $E - P > R$ interval, the salt transport through inflow and outflow became equal while $E - P - R$ was still positive. In the $R > E - P$ interval, the Atlantic inflow is too small to compensate for the outflow while $R > E - P$. Therefore, minimum salinity in the deep basin is reached at the very end of the $R > E - P$ interval, i.e. when $R = E - P$.

The dynamics in the marginal basin are even more complicated. While Atlantic salinity is constant for exchanges between the deep basin and the Atlantic, the deep basinal salinity is variable for exchanges between the marginal and deep basins (Fig. 2F,G). The interaction of interbasinal exchange and the net fresh water budget leads, in this case, to a minimum salinity in the marginal basin 3.700 kyr before the end of the $R > E - P$ interval (which is concomitant with the salinity minimum in the deep basin) and a maximum salinity 1.040 kyr before the end of the $E - P > R$ interval.

Both gypsum and halite concentrations follow the salinity curves in the deep and marginal basins as long as saturation is not reached

(Fig. 2A,B). When saturation is reached, as for gypsum in the marginal basin, the gypsum concentration stabilizes at the saturation concentration while all gypsum in excess of this concentration is deposited. Due to the asymmetrical peak in salinity, the middle of the gypsum deposition interval does not exactly coincide with the highest salinity. However, because the mismatch is relatively small we will consider salinity maxima to coincide with the middle of an interval of gypsum deposition.

Although the exact time of the salinity minimum and maximum may vary depending on the net fresh water budget and the size of the connections between the basins (discussed further in Sections 3.2.2 and 3.2.1 respectively), both deep and marginal basins will reach their salinity maximum in the second half of the $E - P > R$ interval and their salinity minimum in the second half of the $R > E - P$ interval. Therefore, salinity minimum and maximum do not coincide with the precession minimum and maximum in the middle of the $R > E - P$ and $E - P > R$ intervals: a phase lag exists.

3.2. Phase lags during Messinian PLG formation

3.2.1. Sensitivity to gateway size and precessional amplitude

In the previous section the combination of $ampR$, $ampE$, g_{DA} and g_{MD} was chosen for illustrative purposes. In this section, the precession phase of salinity minimum and maximum will be examined in a series of model runs in which $ampR$ and $ampE$, and the size of the two gateways are systematically varied.

Since the aim is to assess the likelihood and magnitude of a phase lag in the PLG evaporites, part of the model results can be discarded because they do not match with observational constraints on the PLG (see also Topper et al., 2014). Evidence of continental water fluxes temporarily lowering salinities to marine or brackish has been found in several marginal basins (Lugli et al., 2010, and references therein). Therefore, we discard results where minimum salinities are $>50 \text{ g/L}$. This directly excludes those results where gypsum saturation continues throughout a precession cycle. Other constraints on the model results derive from the occurrence of gypsum in every precession cycle in the marginal PLG deposits and the lack of halite in both deep and marginal basins. Therefore, gypsum saturation must be reached in the marginal basin in a precession cycle, and halite saturation may not be reached in either basin.

The time, within a precession cycle, when maximum and minimum salinity and gypsum concentration are reached, has been monitored in the last 20 kyr of each 1 Myr run (Fig. 3). Each of the subfigures of Fig. 3 is composed of 4×3 double frames. Each double frame corresponds to a different combination of g_{DA} and g_{MD} . g_{DA} , the connectivity (\approx size) of the Atlantic-deep basin connection, goes down when moving a row of frames up; g_{MD} goes up when moving a column to the right. Within each double frame, the left frame shows the results from the deep basin, the right frame from the marginal basin. Along the vertical axis of every single frame $ampR$ is varied between 0 and 100%; while $ampE$ varies along every horizontal axis between 0 and 50%. The range of g_{DA} in Fig. 3 contains all scenarios where gypsum can be formed; at a higher g_{DA} the larger Atlantic–Mediterranean exchange holds salinities below gypsum saturation. At any g_{MD} larger than the range in Fig. 3, phase lags in deep and marginal basins are the same as those at $g_{MD} = 10^2$ in the deep basin. White stars in each subfigure of Fig. 3 correspond to the minimum and maximum values of Fig. 2A and B.

The coloured ranges in Fig. 3 do comply with all observational constraints, the white areas do not. At low amplitude variations (low $ampR$ and $ampE$), salinity fluctuations within a precession cycle are small and either the minimum salinity is too high or gypsum saturation is not reached. At $g_{MD} = 10^{-1}$, the marginal basin is barely connected to and affected by the deep basin. In this setting, the coloured range is made small by the occurrence of low gypsum concentrations at low amplitudes, and halite saturation at high amplitudes.

As long as gypsum saturation is not reached, gypsum concentrations are proportional to the total salinity. Therefore, gypsum minima (Fig. 3C)

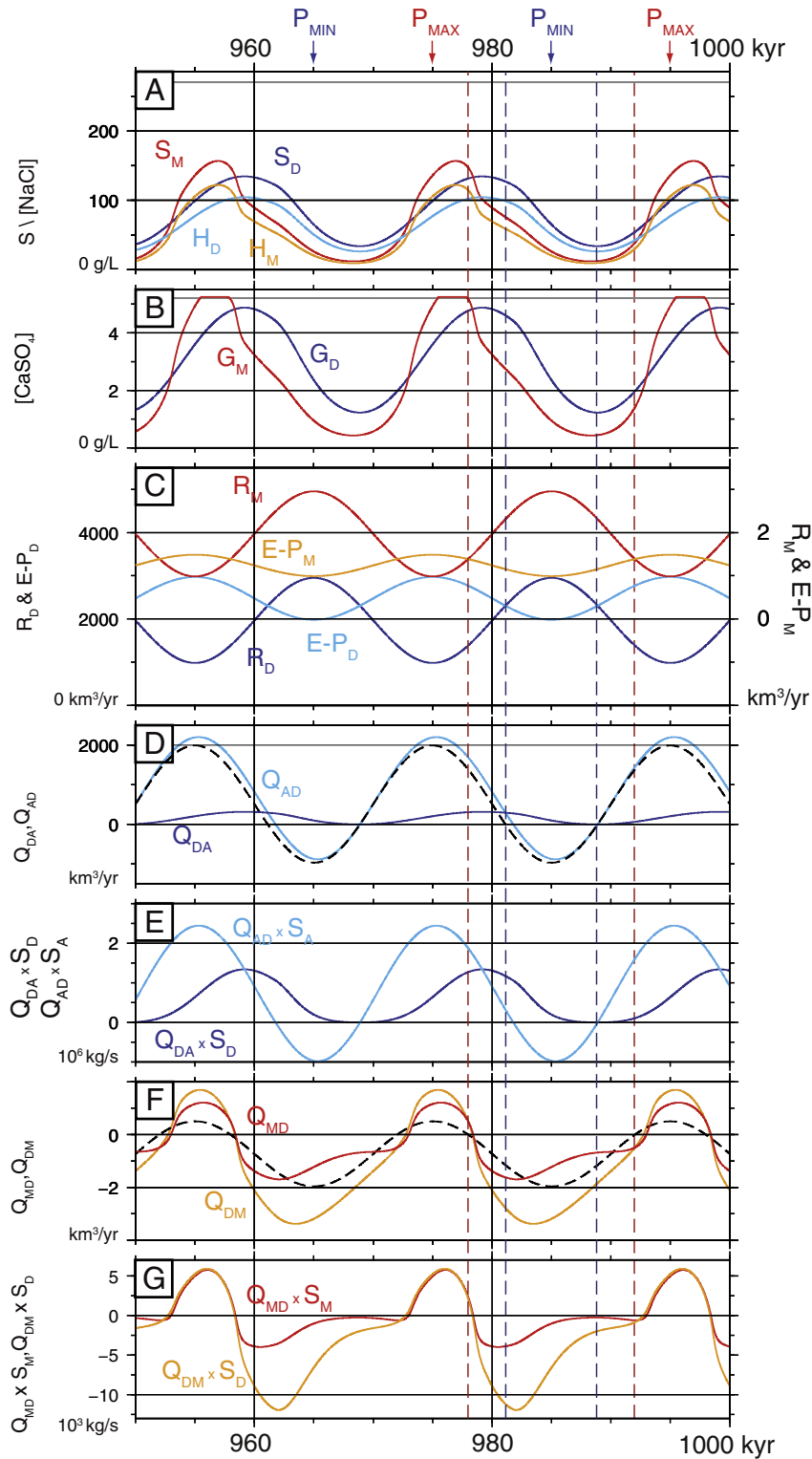


Fig. 2. Evolution of water characteristics and transports in the last 50 kyr of a 1 Myr model run. Shown are (A) salinity and NaCl concentration, (B) CaSO_4 concentration, (C) R and $E - P$, (D) inflow, outflow and net flow (dashed line) in the Atlantic–Mediterranean connection, (E) salt inflow and outflow through the Atlantic–Mediterranean connection, (F) inflow, outflow and net flow (dashed line) in the deep–marginal basin connection, (G) salt inflow and outflow through the deep–marginal basin connection. Grey bars in (A,B) indicate the range of respectively >90% halite and gypsum saturation. Vertical dashed lines indicate the $R > E - P$ interval for the deep (blue) and marginal (red) basin.

are reached at the same time as salinity minima (Fig. 3A). In the parameter range of Fig. 3, salinity minima in marginal and deep basins are reached respectively 2.5–4.5 and 3–4.5 kyr after the precession minimum, salinity maxima respectively 1–6 and 3–6.5 kyr after the

precession maximum. The timing of gypsum maxima represents the time that gypsum saturation is reached and deposition commences, from 1.5 kyr before up to 4.5 kyr after the precession maximum.

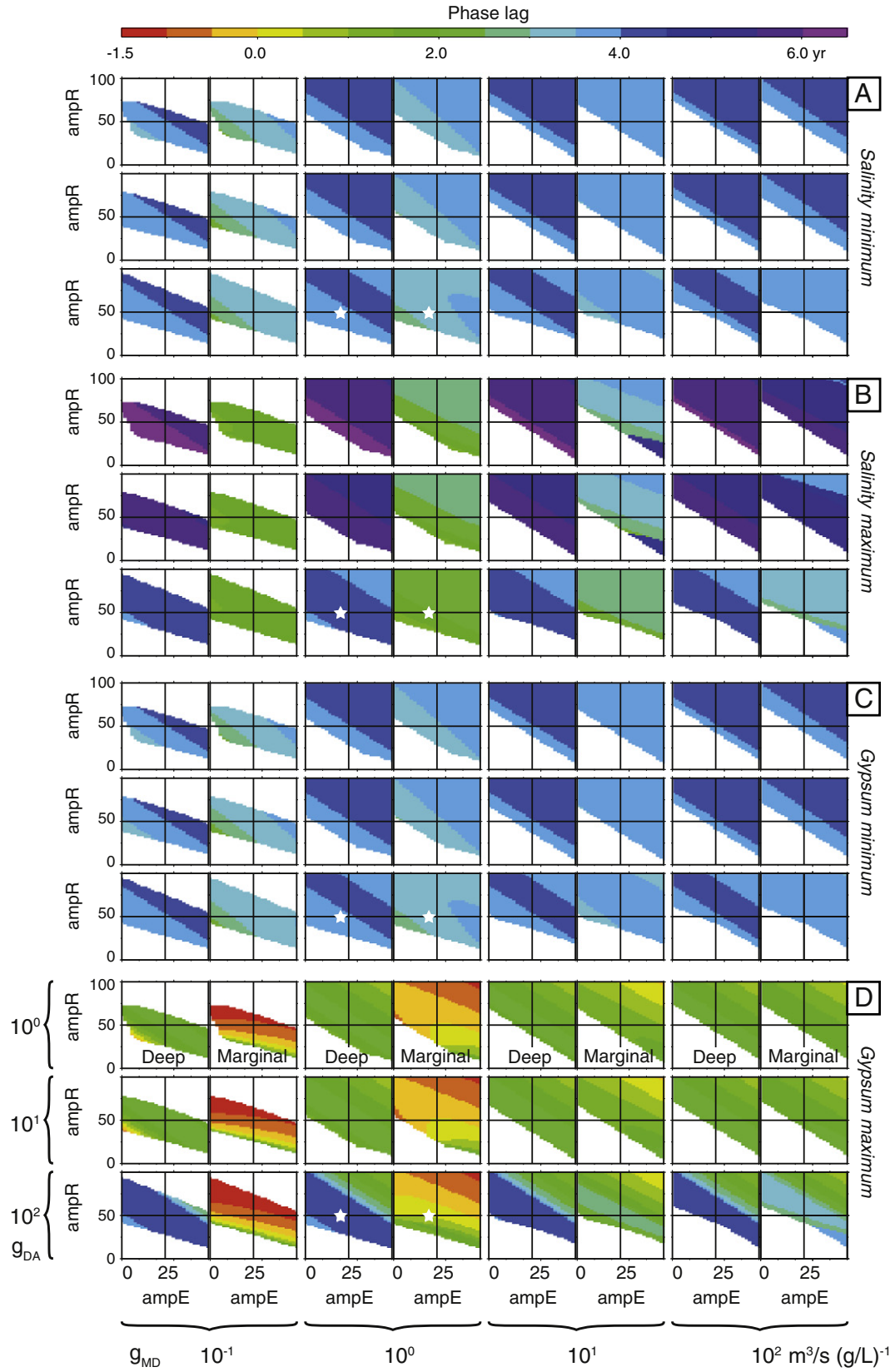


Fig. 3. Precessional phase lag of minimum (A) and maximum (B) salinity and minimum (C) and maximum (D) gypsum concentration. Coloured areas contain the scenarios that fit all observations for the PLG phase, white areas the scenarios where one or more constraints are not met. The locations of minimum and maximum values from Fig. 2 are indicated with white stars in the corresponding subfigure.

The similarity in colour and pattern between the different rows in Fig. 3A indicates that the size of the Atlantic–Mediterranean connection has hardly any effect on the timing of salinity minima. In the salinity maxima (Fig. 3B), on the contrary, a relatively small but significant change is visible: maxima are reached further from the precession maximum at lower g_{DA} . This is because, at low g_{DA} , the salt influx from the inflow is only compensated by the smaller outflow when sufficiently high salinities are reached ($Q_{AD} \cdot S_A = Q_{DA} \cdot S_D$) closer to the end of the $E - P > R$ interval.

Where exchange with the deep basin is relatively large ($g_{MD} \geq 10^2$), it keeps water characteristics in the two basins close to each other and phase lags in both basins are similar. In the deep basin, the interval with $E - P > R$ shortens towards higher amplitudes (Fig. 4), e.g. moving from bottom-left to top-right in a single frame. However, at higher amplitudes the length of the $E - P > R$ interval stabilizes (Fig. 4). Consequently, the time at which maximum concentrations are reached, shifts towards the precession maximum in the $ampR$ – $ampE$ range where the length of the interval decreases (Fig. 3). The time of minimum concentrations, accordingly, shifts away from the precession minimum at higher amplitudes. Contrary to the deep basin where the precession-averaged fresh water budget is negative, the marginal basin fresh water budget is on average positive. A shift to higher amplitudes therefore lengthens the interval with $E - P > R$ (Fig. 4). This would result in an opposite trend, compared to the deep basin, if interbasinal exchange didn't play a role. Nevertheless, maxima/minima in the marginal basin are reached closer to the precession maximum/minimum compared to the deep basin (Fig. 3). When the marginal basin is less affected by exchange with the deep basin, at lower g_{MD} , maxima and minima are closer to the corresponding precession peak.

In the time of onset of gypsum deposition in the marginal basin (Fig. 3D), three trends are visible: deposition starts earlier in the precession cycle with (1) a smaller Atlantic–Mediterranean connection, (2) a smaller deep–marginal basin connection, and (3) at larger $ampR$ and $ampE$. With a smaller Atlantic–Mediterranean connection, salinity rises faster in the Mediterranean when $E - P > R$. Therefore, gypsum saturation is reached closer to the start of the $E - P > R$ interval. With a smaller deep–marginal basin connection, salinity rises faster in the

marginal basin when the marginal fresh water budget is negative ($E - P > R$). On the other hand, the greater influence of the marginal fresh water budget will cause a reduction of the duration of gypsum deposition because the marginal $E - P > R$ interval is shorter than that of the deep basin. At larger $ampR$ and $ampE$, $E - P - R$ becomes larger, leading yet again to a faster salinity rise in the $E - P > R$ interval.

3.2.2. Sensitivity to water column stratification and fresh water budget

Water column stratification, inferred to have affected the facies of marginal PLG deposits and to impede deep basin gypsum deposition (de Lange and Krijgsman, 2010; Lugli et al., 2010), has not been discussed in the previous sections because it would further complicate the explanation of the basic dynamics of the system. Also, the average fresh water budget has been kept constant at $fR_M = fR_D = 1.5$, a value derived from previous studies (Topper et al., 2011; Topper and Meijer, 2013).

An increasing water column stratification leads to higher deep water salinities (not shown here, but a more extensive and detailed examination of the sensitivity of the results to the fresh water budget and water column stratification can be found in Topper (2013)). Compared to experiments without stratification, the range that fits the observational constraints is smaller because the higher salinity reduces the range that reaches a low enough salinity and increases the range where halite is reached. Furthermore, maximum salinities are reached closer, on average a few hundred years, to the precession maximum. Besides that, results are comparable; water column stratification does not have a major influence on the phase lag of salinity.

In order to examine the sensitivity of the phase lag to stratification and the average fresh water budget, both have been varied systematically in a large number of model runs. In short, the phase lag of salinity minima increases towards higher fR_D and fR_M due to a longer $R > E - P$ interval (Fig. 4); the phase lag of salinity maxima increases towards lower fR_M , due to a longer $E - P > R$ interval (Fig. 4), and higher fR_D , due to lower deep basin salinity. In all model results that comply with the observational constraints for the PLG, salinity minima as well as maxima always occur after the corresponding precession peak.

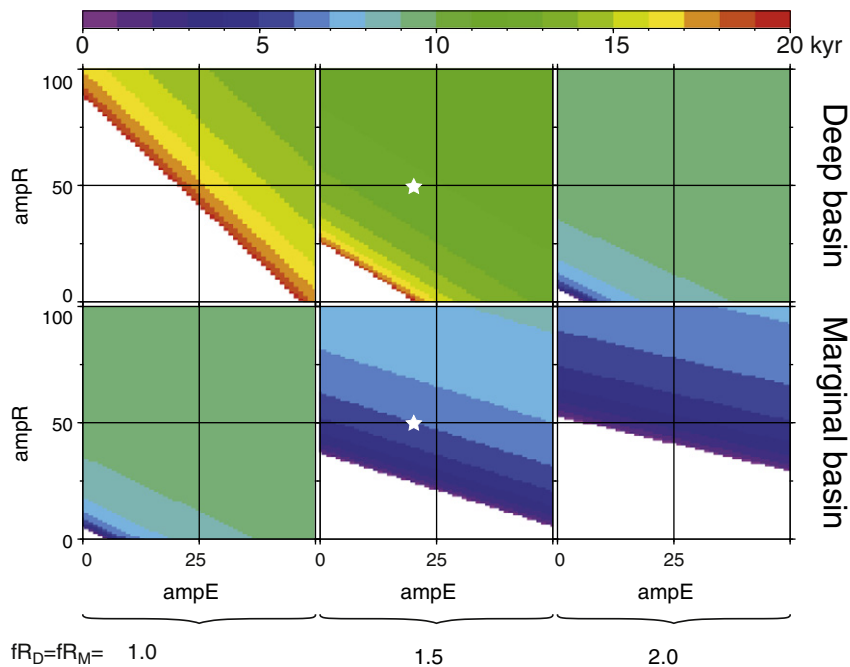


Fig. 4. Duration of the $E - P > R$ interval in the deep basin (top row) and marginal basin (bottom row) for different fR : $fR_D = fR_M = 1.0$ (left), $fR_D = fR_M = 1.5$ (middle), $fR_D = fR_M = 2.0$ (right). The areas of the $ampR$ – $ampE$ range where either $E - P$ exceeds R or R exceeds $E - P$ during the whole precession cycle are white. White stars correspond to the $ampR$ – $ampE$ combination used in Fig. 2.

3.2.3. Sensitivity to precession cycle length

Although the foregoing sections have focussed on a climatic precession cycle with an idealized length of 20 kyr, the cycle length, i.e. precession modulated by eccentricity and obliquity, during the PLG phase varied between 14 and 33 kyr. Both the shortest, which is the cycle after the onset of the MSC, and the longest cycles coincide with eccentricity minima. In contrast with eccentricity maxima during which the cycle length is quite constant at ≈ 20 kyr, it varies considerably during eccentricity minima (Huybers and Aharonson, 2010). To assess how much the phase lag of salinity extrema differs between cycles with different lengths the model has been run for ≈ 4 million combinations of fR_D , fR_M , g_{DA} , g_{MD} , $ampE$, $ampR$ for 11 different cycle lengths in the range 10 to 30 kyr. For every cycle length the phase lags of the salinity extrema in the marginal basin from the results that fit all observational constraints have been sorted in 100 year bins (Fig. 5). Plotted for each bin is the percentage of the runs that fit all observational constraints within that bin. For example, for a cycle length of 20 kyr 1.8% of the results that fit the observational constraints have a phase lag of 2000 ± 50 years in the salinity maximum (Fig. 5B), i.e. a phase lag in the salinity maximum similar to that shown in Fig. 2. The percentages in all bins add up to 100% for every cycle length. Also indicated are the minimum, maximum and average phase lags for each cycle length.

For both the salinity minimum and salinity maximum the average phase lag increases when the cycle becomes longer. Furthermore, the range of phase lags also increases because of a shift to larger maximum

phase lags. Minimum phase lags are, regardless of the duration of the cycle, in the order of a few hundred years, maximum phase lags are approximately 30% of the duration of the cycle. At different cycle lengths the distribution of the phase lags is different. While for a cycle of 10 kyr the phase lags of the salinity minimum are concentrated near 1.7 kyr, the phase lags for a 30 kyr cycle are unevenly spread out around 5.2 kyr. In the phase lag distribution of the salinity minimum in cycles > 18 kyr two peaks are visible. These two peaks are more clear in the salinity maximum phase lags distribution, and even clearer in the distribution of the phase lags in the deep basinal salinity extrema (Fig. 7). These two peaks reflect the difference in phase lags between results from experiments with a relatively large and those with a small connection to the Atlantic ($g_{DA} = 10^2$ vs $g_{DA} \leq 10^1$, e.g. in Fig. 3). This difference is most pronounced in long cycles but, although significantly smaller, is also present in shorter cycles.

Compared to the phase lag distribution of the deep basin (Fig. 7) phase lags in the marginal basin are on average smaller. This is mainly caused by the small volume of the marginal basin; changes in the fresh water budget or exchange with the deep basin cause more rapid changes of water characteristics when the fluxes are large compared to the basinal volume. Hence, extrema are usually reached closer to the precession peaks than in the deep basin. The phase lag distributions of the salinity minimum in the marginal basin are similar to those of the deep basin whereas the phase lag distributions of the salinity maximum are clearly different. Due to the relatively large interbasinal exchange

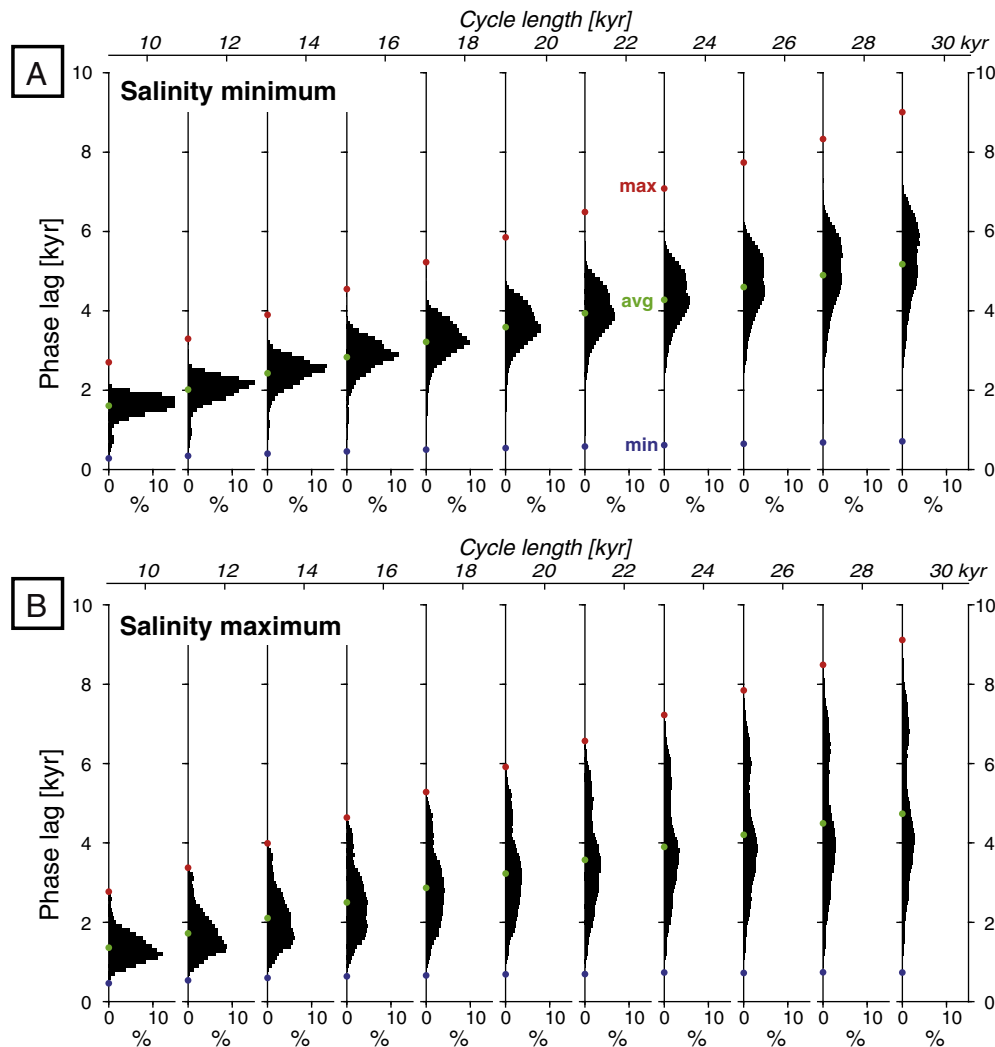


Fig. 5. Distribution of phase lags in the salinity (A) minimum and (B) maximum in the marginal basin for different cycle lengths. From all results that fit the observational constraints the phase lags have been sorted in bins of 100 years. The value for a bin is expressed as the percentage of all results that fit the observational constraints in that specific bin.

after the precession minimum salinity minima in the deep and marginal basin are generally close together. On the other hand, the marginal and deep basin behave more independently after the precession maximum which results in more variation in the phase lags of both basins. Furthermore, when the marginal-deep basin connection is strongly restricted the marginal basin will behave almost independently from the deep basin and phase lags in both basins may differ notably. This is visible in the larger range of phase lags in the marginal basin phase lag distributions compared to the deep basin phase lag distributions.

In summary, the phase lags of the salinity extrema are larger when the cycle is longer. However, the average phase lag does not scale linearly to cycle length. The average phase lag in the deep basin is larger while the range of phase lags is significantly larger for the marginal basin.

4. Discussion

In all results of the model set up to represent the Mediterranean during PLG formation, a phase lag exists between the precession minimum/maximum and the minimum/maximum salinity. The large range of settings examined, confirms that it is a robust result. The systematic offset between the precession signal and the extrema in salinity calls for a revision of our perception of the link between the precession signal and its sedimentary expression. Accordingly, the astronomical tuning of the PLG deposits and the timing of the MSC onset should be reconsidered (Fig. 6).

Since cyclostratigraphy was first used to resolve the onset and timing of the MSC stages, precession maxima have been correlated with the evaporite layers in the PLG, and precession minima with the

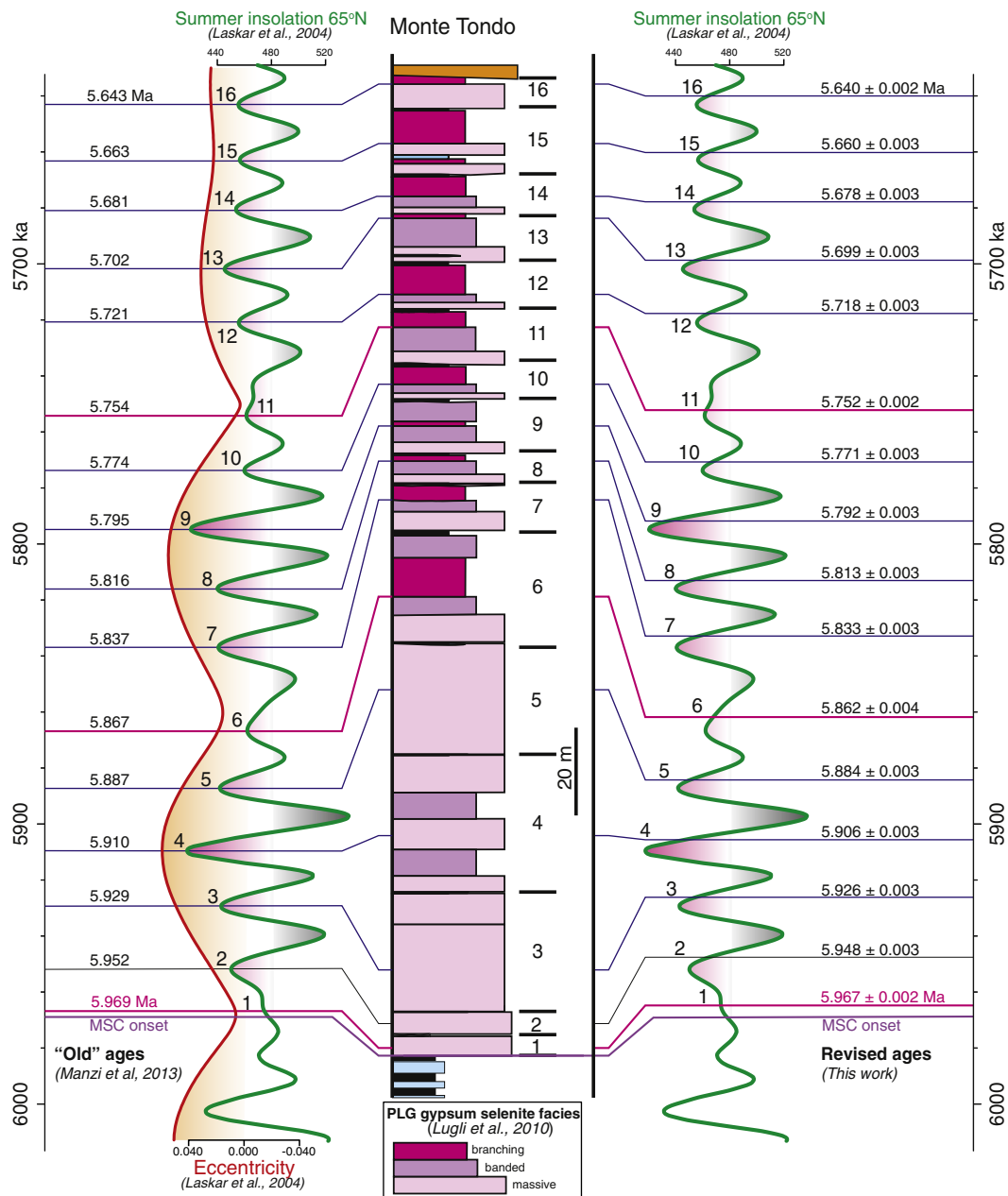


Fig. 6. Revised tuning of the Primary Lower Gypsum unit. The stratigraphic column of the Monte Tondo section is the most complete PLG sequence. On the left the ages assigned to the gypsum midpoints (salinity maxima) by Manzi et al. (2013), on the right the revised ages from this work. New ages represent the old ages plus the cycle length dependent average phase lag. The indicated error is solely phase lag related.

intercalated shale layers (e.g. Krijgsman et al., 1999; Manzi et al., 2013). A correlation similar to that used for the marl-sapropels deposits of the pre-MSC. According to the facies interpretation of Lugli et al. (2010), banded selenites are associated with the highest degree of saturation, i.e. the highest salinity, during a precession cycle. However, when massive selenite is the only gypsum facies formed in a precession cycle (cycles 1–5, Fig. 6), its time of deposition with respect to the time of highest saturation – in their interpretation at the precession maximum – is unclear. In Figs 12 and 13 of Lugli et al. (2010), respectively the middle and the top of the massive selenite coincide with the highest saturation. Because it makes sense to have gypsum formation at the peak salinity, a correlation of the middle of massive selenite layers, when other facies are absent, with the highest salinity during a precession cycle seems appropriate and has been applied in Fig. 6.

It follows from our analysis that, although the exact timing may vary dependent on fresh water budgets and gateway sizes, the highest salinity in a precession cycle cannot be correlated with the precession maximum. If the fresh water budget and connectivity to the deep basin are known for a marginal basin of which PLG is used for cyclostratigraphic dating, the correlation between the precession signal and the deposits can be determined from model results. In the more realistic case that these marginal basin characteristics are unknown, we propose that a phase lag of 0.7–5.9 kyr should be taken into consideration for a 20 kyr precession cycle. It follows that even if a phase lag of 3.3 kyr is reckoned with – 3.3 kyr being the average phase lag in a representative set of experiments (Fig. 5) – an error margin of 2.6 kyr must be added.

Even though the possible range of phase lags is large, our results show that the phase lag will be lower in a low amplitude precession cycle (low *ampE* and *ampR*) than in a high amplitude precession cycle (Fig. 3). It is lower as well when either or both of the connections between the Mediterranean and Atlantic (g_{DA}) and between the marginal and deep basins (g_{MD}) is larger. The same parameters that affect the phase lag, affect the time of onset of gypsum formation in the marginal basin as well. Gypsum thicknesses are expected to be higher in high amplitude precession cycles with a small Atlantic–Mediterranean connection and a small marginal–deep basin connection. A more detailed analysis by (Topper et al., 2014) also shows these trends.

Starting from the onset of the MSC we have determined the length of the PLG cycles by calculating the time from a midpoint of insolation maximum and insolation minimum, like the MSC onset, to the next midpoint in the La2004 summer insolation at 65°N (Laskar et al., 2004). All cycles during PLG formation have a duration of 18–23 kyr apart from two anomalously long cycles of 29 and 33 kyr and a short cycle of just 14 kyr after the onset of the MSC. For the 18–23 kyr cycles a phase lag of $3-4 \pm 3$ kyr is suggested by our model results (Fig. 5). Accordingly, ages for the midpoints of the massive selenite or branching selenite are equal to the age of the insolation minimum + 3–4 kyr with an uncertainty of 3 kyr (Fig. 6). For the 29 and 33 kyr cycles this increases to 5 kyr with an uncertainty of 4 kyr. However, if we consider cycle 11 as being composed of two cycles of respectively 14 and 19 kyr, the phase lag would be just 2 kyr with an uncertainty of 2 kyr.

During periods of low eccentricity the length of insolation cycles varies much more than in periods of high eccentricity (Huybers and Aharanson, 2010). The onset of the MSC falls in such a period with low eccentricity. The cycle after the onset of the MSC is just 14 kyr and the time between the two insolation minima before and after the onset of the MSC is just 12 kyr. The mechanisms responsible for the phase lag as described for the 20 kyr cycle in this study, also act in longer and shorter cycles. The phase lag, unfortunately, does not scale linearly with the length of the precession cycle. For example, a model with settings equal to those used for Fig. 2 and a 12 kyr shows a phase lag of the salinity maximum of only 1110 yr, vs 4170 yr in the 20 kyr cycle. A further examination of the influence of the length of the precession cycle on the phase lag shows that the average phase lag in a 12 kyr precession cycle is 1.7 kyr (range: 0.5–3.4 kyr), i.e. comparable in

magnitude with the other uncertainties of astronomical tuning. Nevertheless, taking into account the phase lag of the gypsum midpoint with respect to the insolation peak, the onset of the MSC is a (few) kyr more recent than that inferred by Manzi et al. (2013).

Due to the short precession cycle spanning the onset of the MSC and the inherent small phase lag, the correlation of the MSC onset with an interval characterized by glacial conditions as proposed by Hodell et al. (1994), and recently again by Manzi et al. (2013), is not compromised by our results. Also, the correlation of the MSC phase with halite deposition with glacial intervals TG12 and TG14 is upheld. However, a phase lag of a few kyr is predicted between the peak glacial conditions and halite formation.

In the previous sections, we have considered the phase lag of the maximum salinity peak, which approximately coincides with the middle of a gypsum layer, instead of the phase lag of the onset of gypsum formation. Because of the large time interval in which gypsum saturation may be reached within a precession cycle, the base of a gypsum layer is hard to date and hence not a suitable alternative for the use of the middle of a massive selenite or banded selenite.

The sapropels of the pre-MSC formed in a far more restricted Mediterranean basin than more recent sapropels. If they and the shale intercalations of the PLG formed, respectively, near the lowest salinities and in the interval without gypsum formation, their midpoints cannot be correlated with a precession minimum. Because the setting of pre-MSC sapropel formation does not fit the observational constraints for the PLG these results are not shown in the figures. Again, the exact timing is dependent on fresh water budgets and gateway size, but salinity minima occur 1–6 kyr after the precession minimum in a 20 kyr precession cycle. If the sedimentation rate was constant during shale formation and sapropels formed near the minimum salinity (Flores et al., 2005), a phase lag of 1–6 kyr, with an average at 3.6 kyr, should be reckoned with according to our results. Phase lags for shorter and longer cycle lengths can be found in Fig. 5.

5. Conclusions

The phase relation between precession-driven climate change and the sedimentary expression is an important but largely unknown factor in astronomical tuning. The precession-paced deposition of evaporites in the Mediterranean during the Messinian Salinity Crisis is easily captured in a simple box model. Hence, the Messinian Mediterranean is a convenient setting to study precessional phase lags. In an extensive sensitivity analysis with a box model, a consistent phase lag is found between the precessional forcing and salinity minima and maxima in the marginal and deep basins of the Mediterranean.

In a precession cycle with a duration of 20 kyr, the modelled precessional phase lag of the salinity maximum in a Mediterranean marginal basin is 0.7–5.9 kyr, with an average at 3.3 kyr. The modelled salinity maximum can be correlated with the transition from massive to banded selenite or the middle of a massive selenite layer when other facies are not present within a precession cycle.

In cycles with a duration of less or more than 20 kyr, the phase lag is respectively shorter and longer. The magnitude of the phase lag of the salinity maximum does not scale linearly with the length of the cycle: 1.4 kyr (range: 0.5–2.8 kyr) for a 10 kyr cycle, up to 4.8 kyr (range: 0.7–9.1 kyr) for a 30 kyr cycle.

Because the precession cycle spanning the onset of the MSC is anomalously short, a phase lag will not significantly affect the timing of the onset of the MSC. For the astronomical tuning of the other gypsum deposits, we propose that a phase lag of 3.3 kyr (± 2.6 kyr) should be taken into account for 20 kyr precession cycle, i.e. the astronomically tuned ages become 3.3 kyr younger, and a lower and higher phase lag for respectively shorter and longer precession cycles.

Supplementary data to this article can be found online at <http://dx.doi.org/10.1016/j.palaeo.2014.10.025>.

Acknowledgements

We would like to thank Christian Zeeden, Rick Hennekam and Rinus Wortel for their valuable discussions and comments to the manuscript. RPMT is supported by the Netherlands Research Center for Integrated Solid Earth Science. Computational resources for this work were also provided by ISES (ISES 3.2.5 High End Scientific Computation Resources). Figures in this paper were created using GMT version 4.5.1 (Wessel and Smith, 1991).

References

- Adloff, F., Mikolajewicz, U., Kucera, M., Grimm, R., Maier-Reimer, E., Schmiedl, G., Emeis, K.C., 2011. Upper ocean climate of the Eastern Mediterranean Sea during the Holocene Insolation Maximum—a model study. *Clim. Past* 7, 1149–1168.
- CIESM, 2008. The Messinian Salinity Crisis from mega-deposits to microbiology – a consensus report. CIESM Workshop Monographs N° 33.
- de Lange, G., Krijgsman, W., 2010. A unifying mechanism for shallow gypsum and deep dolomite formation during the Messinian Salinity Crisis. *Mar. Geol.* 275, 273–277.
- Flores, J.A., Sierro, F.J., Filippelli, G.M., Bárcena, M.A., Pérez-Folgado, M., Vázquez, A., Utrilla, R., 2005. Surface water dynamics and phytoplankton communities during deposition of cyclic late Messinian sapropel sequences in the western Mediterranean. *Mar. Micropaleontol.* 56, 50–79.
- Gladstone, R., Flecker, R., Valdes, P., Lunt, D., Markwick, P., 2007. The Mediterranean hydrologic budget from a Late Miocene global climate simulation. *Palaeogeogr. Palaeoclimatol. Palaeoecol.* 251, 254–267.
- Grimm, R., 2012. Simulating the early Holocene eastern Mediterranean sapropel formation using an ocean biogeochemical model (Ph.D. thesis) Reports of Earth system Science No 123. Max Planck Institute for Meteorology, Hamburg, Germany.
- Hodell, D.A., Benson, R.H., Kent, D.V., Boersma, A., Rakic-El Bied, K., 1994. Magnetostratigraphic, biostratigraphic, and stable isotope stratigraphy of an Upper Miocene drill core from the Salé Briqueterie (northwestern Morocco): a high-resolution chronology for the Messinian stage. *Paleoceanography* 9, 835–855.
- Huybers, P., Aharanson, O., 2010. Orbital tuning, eccentricity, and the frequency modulation of climatic precession. *Paleoceanography* 25 (PA4228).
- Kouwenhoven, T.J., van der Zwaan, G.J., 2006. A reconstruction of late Miocene Mediterranean circulation patterns using benthic foraminifera. *Palaeogeogr. Palaeoclimatol. Palaeoecol.* 238, 373–385.
- Krijgsman, W., Hilgen, F.J., Raffi, I., Sierro, F.J., Wilson, D.S., 1999. Chronology, causes and progression of the Messinian Salinity Crisis. *Nature* 400, 652–655.
- Kutzbach, J.E., Liu, X., Liu, Z., 2008. Simulation of the evolutionary response of global summer monsoons to orbital forcing over the past 280,000 years. *Clim. Dyn.* 30, 567–579.
- Laskar, J., Robutel, P., Joutel, F., Gastineau, M., Correia, A.C.M., Levrard, B., 2004. A long-term numerical solution for the insolation quantities of the earth. *Astron. Astrophys.* 428, 261–285.
- Leeder, M., 1999. *Sedimentology and sedimentary basins: from turbulence to tectonics*. Blackwell Science, (592 pp.).
- Lourens, L.J., Antonarakou, A., Hilgen, F.J., Van Hoof, A.A.M., Vergnaud-Grazzini, C., Zacharias, W.J., 1996. Evaluation of the Plio-Pleistocene astronomical timescale. *Paleoceanography* 11, 391–413.
- Lugli, S., Manzi, V., Roveri, M., Schreiber, B.C., 2010. The Primary Lower Gypsum in the Mediterranean: a new facies interpretation for the first stage of the Messinian salinity crisis. *Palaeogeogr. Palaeoclimatol. Palaeoecol.* 297, 83–99.
- Manzi, V., Gennari, R., Hilgen, F., Krijgsman, W., Lugli, S., Roveri, M., Sierro, F.J., 2013. Age refinement of the Messinian salinity crisis onset in the Mediterranean. *Terra Nova* 1–8.
- Meijer, P.Th., 2006. A box model of the blocked-outflow scenario for the Messinian Salinity Crisis. *Earth Planet. Sci. Lett.* 248, 486–494.
- Meijer, P.Th., Slingerland, R., Wortel, M.J.R., 2004. Tectonic control on past circulation of the Mediterranean Sea: a model study of the Late Miocene. *Paleoceanography* 19, 1–19 (PA1026).
- Rivera, T.A., Storey, M., Zeeden, C., Hilgen, F.J., Kuiper, K., 2011. A refined astronomically calibrated $^{40}\text{Ar}/^{39}\text{Ar}$ age for Fish Canyon sanidine. *Earth Planet. Sci. Lett.* 311, 420–426.
- Topper, R.P.M., 2013. A model analysis of atypical marine sedimentation in mediterranean basins (Ph.D. thesis) Utrecht Studies in Earth Sciences No. 46. Department of Earth Sciences, Utrecht University.
- Topper, R.P.M., Flecker, R., Meijer, P.Th., Wortel, M.J.R., 2011. A box model of the Late Miocene Mediterranean Sea: implications from combined $^{87}\text{Sr}/^{86}\text{Sr}$ and salinity data. *Paleoceanography* 26 (PA3223).
- Topper, R.P.M., Manzi, V., Lugli, S., Roveri, M., Meijer, P.Th., 2014. Precessional control of Sr ratios in marginal basins during the Messinian Salinity Crisis. *Geochim. Geophys. Geosyst.* 15, 1926–1944.
- Topper, R.P.M., Meijer, P.Th., 2013. A modelling perspective on spatial and temporal variations in Messinian evaporite deposits. *Mar. Geol.* 336, 44–60.
- Tuenter, E., Weber, S.L., Hilgen, F.J., Lourens, L.J., 2005. Simulation of climate phase lags in response to precession and obliquity forcing and the role of vegetation. *Clim. Dyn.* 24, 279–295.
- Weber, S.L., Tuenter, E., 2011. The impact of varying ice sheets and greenhouse gases on the intensity and timing of boreal summer monsoons. *Quat. Sci. Rev.* 30, 469–479.
- Wessel, P., Smith, W.H.F., 1991. Free software helps map and display data. *EOS Trans. AGU* 72, 441–446.
- Ziegler, M., Tuenter, E., Lourens, L.J., 2010. The precession phase of the boreal summer monsoon as viewed from the eastern Mediterranean (ODP Site 968). *Quat. Sci. Rev.* 29, 1481–1490.